Journal of Sound and Vibration (2000) **231**(1), 145–173
doi:10.1006/jsvi.1999.2673, available online at http://www.idealibrary.com on IDEAL®

A STUDY OF THE LIMIT CYCLES ASSOCIATED WITH A GENERALIZED CODIMENSION-3 LIENARD OSCILLATOR

W. ZHANG† AND P. YU

Department of Applied Mathematics, The University of Western Ontario, Ontario, Canada N6A 5B7

(*Received* 21 *July* 1999 *and in final form* 8 *September* 1999)

In this paper Melnikov and Petrov methods are used to study the limit cycles associated with the degenerate bifurcations of a representative, generalized codimension-3 Lienard oscillator. It is shown that the coexistence of multiple limit cycles is possible and that jumping phenomena exist between limit cycles. Moreover, it is found that the stable limit cycles (oscillations) and the unstable limit cycles (oscillations) can occur alternatively.

1. INTRODUCTION

Many engineering problems are related to non-linear self-excited vibrations, for example, the self-excited oscillations in bridges and airplane wings, the beating of a heart, the non-linear model of machine tool chatter [1], the vortex- or flow-induced oscillations in the cylinder of square cross-section [2, 3], the galloping of transmission lines [4–6], etc. In the above-mentioned reports, non-linear oscillation models are established based on the characteristics of the engineering problems. One of the earliest work on the problem of machine tool chatter was reported by Arnold [7] in which a self-excited non-linear oscillator model was proposed:

$$M\ddot{x} - [A - Bx - \phi(x)]\dot{x} + F'x = K,$$

where M, A, B, F′ and K are constants, and $\phi(x)$ is an unspecified function that represents the dependence of system damping on the machine tool motion x. If the friction effects between the workpiece and the machine tool as well as between the chip and machine tool are considered, a one-degree-of-freedom model was obtained [8]:

$$m\ddot{y} + \left[C - C_e\left(\frac{1}{1 - \dot{y}/v_0}\right)\right]\dot{y} + (k - k_e)y = 0,$$

†Permanent address: College of Mechanical Engineering, Beijing Polytechnic University, Beijing 100022, China.

0022-460X/00/110145 + 29 $35.00/0

where m, C, C_e, k, k_e are constants and v_e is the constant velocity with which the workpiece moves past the tool.

Another example is the simple galloping model of cables, described by one-degree-of-freedom non-linear oscillator [9]:

$$m\ddot{y} + \left[2m\varsigma\omega_y - \frac{1}{2}\rho U^2 D\,\frac{\partial C_y(\dot{y}=0)}{\partial \dot{y}}\right]\dot{y} + ky = 0,$$

where ς, ρ, U and C_y are the linear damping ratio, the density of air, the steady wind speed and the aerodynamic force, respectively.

However, it is noted in the above three equations that non-linearity is only involved in the damping terms. In fact, many physical systems also have non-linearity included in stiffness terms. For example, the non-linear oscillator considered in reference [10] is described by

$$\ddot{x} + 0{\cdot}03\dot{x}|\dot{x}| + 4\pi^2 \sin x = 0,$$

which exhibits periodic solutions.

This indeed shows that many engineering oscillation problems can be modelled by a one-degree-of-freedom self-excited non-linear oscillator, which may be represented by the generalized codimension-3 Lienard oscillator:

$$\ddot{x} - [2\bar{\mu} - 2\alpha x^2 + (6\gamma - 4\alpha\beta)x^4]\dot{x} - \bar{\sigma}x + \tfrac{3}{2}\beta x^3 = 0, \tag{1}$$

where α, β, μ, γ and $\bar{\sigma}$ are parameters. A great concern in the study of such a model is the possible periodic solutions (limit cycles) and their stability. This may give rise to phenomena such as coexistence of multiple limit cycles and jumping.

An important research task related to a study of limit cycles is to find the maximum number of the limit cycles. This is, in general, not easy due to the difficulty in finding the relationship between the zeros of a Melnikov function and the number of the limit cycles. This problem has been discussed by many researchers, some of them focused on the Lienard oscillator. For example, Giacomini and Neukirch [11] used a sequence of polynomials to find the number and location of limit cycles. Sanjuan [12] established the relationship between the Melnikov theory and the number of limit cycles, while Mickens [13] applied the Melnikov theory to discuss the number of the limit cycles. Burnette and Mickens [14], on the other hand, investigated the number of limit cycles for a generalized mixed Rayleigh–Lienard oscillator.

This paper is mainly focused on the study of degenerate bifurcations and limit cycles for the generalized codimension-3 Lienard oscillator. Studying degenerate bifurcations is, in general, more complicated. In 1970s, Takens [15–17] and Bogdanov [18, 19] developed a normal form theory for the degenerate bifurcations of codimension-2 systems, which laid the foundation for further studies on higher codimension degenerate bifurcations. Dumortier *et al.* [20, 21] considered the unfolding and degenerate bifurcations of codimension-3 systems associated with the cusp, saddle, focus and elliptic singularities. Since a codimension-3 system involves three unfolding parameters, the bifurcation diagrams should be shown in a three-dimensional parameter space, and this is not an easy task. Therefore, the key problems in the study of degenerate bifurcations are: how to best represent

bifurcation diagrams, how to find the equations of bifurcation curves and surfaces, and how to determine the bifurcations of the multiple limit cycles. Dumortier *et al.* [20] made a first attempt to solve these problems, and later Li and Rousseau [22, 23] made some important contributions to the study of degenerate bifurcations for codimension-4 systems associated with cusp as well as codimension-3 systems with Z_2-symmetry. They showed that the degenerate bifurcations of higher codimension systems are more complicated compared with other non-degenerate bifurcations.

In the last decade, further studies have been concentrated on degenerate bifurcations of even higher codimension systems as well as on the computation of normal forms. For example Joyal [24] studied degenerate bifurcations of codimension N associated with cusp, but he did not give bifurcation diagrams. Dangelmayr and Guckenheimer [25] analyzed codimension-3 and 4 non-linear dynamical systems with four parameters in planar vector field and used Macsyma to compute normal forms. Sethna and Shaw [26] considered the non-linear oscillations induced by the motion of articulated tubes conveying a fluid, which is actually a degenerate bifurcation problem of codimension 3. Bi and Yu [27] used the Maple program to compute the normal forms for semi-simple cases and gave the application to high-dimensional non-linear dynamical systems. Zhang [28] considered higher order normal forms and analyzed the degenerate bifurcations of codimension 3 for a non-linear dynamical system with Z_2-symmetry. Bi and Yu [29] developed a user-friendly symbolic program using Maple for computing the normal forms of non-linear systems with non-semisimple zero eigenvalues. The program was used to study bifurcations of codimension-3 double-pendulum system. Also, Yu and Bi [30] used the theory of normal forms to consider bifurcations of a double pendulum with a simple zero and a pair of purely imaginary eigenvalues as well as two pairs of purely imaginary eigenvalues.

In order to study the degenerate bifurcations and limit cycles of higher codimension physical problems, first we need to compute the normal form of the system, and in particular, to find the explicit relation between the coefficients of the normal form and that of the original system. Then we determine the universal unfolding of the system and find the relation between the unfolding parameters and parameters of the original system. Finally, we apply Melnikov's and Petrov's methods to study the bifurcation characteristics, of the universal unfolding and identify the regions where homoclinic bifurcation, heteroclinic bifurcation and multiple limit cycles may occur. For a complicated non-linear dynamical system, it is not easy to find the universal unfolding. Thus, we may use an unfolding, instead of the universal unfolding, to analyze the bifurcation characteristics of the system, and may obtain some interesting results which though might not be complete. Sethna and Shaw [26] actually employed this idea to obtain the results of the degenerate bifurcations of codimension-3 on articulated tubes conveying a fluid.

In this paper, based on equation (1), we will investigate the degenerate bifurcations and the limit cycles of the system. Although some results about the number of limit cycles for the Lienard oscillator have been given in references [11–14], it seems that they are not complete. This motivates us to perform a further study on the degenerate bifurcations of the system (1) and find some new interesting results.

Since the dynamical behavior of system (1) is qualitatively different when the parameters β and $\bar{\sigma}$ take different signs, we separate the two cases and present the results for the positive β and $\bar{\sigma}$ in the next three sections, and the results for the negative case in section 5.

2. HOMOCLINIC BIFURCATION

Suppose that $\beta > 0$, $\bar{\sigma} > 0$; setting $u = x$, $v = \dot{x}$ in system (1) yields the normal form

$$\begin{aligned} \dot{u} &= v, \\ \dot{v} &= \bar{\sigma}u - \tfrac{3}{2}\beta u^3 + [2\bar{\mu} - 2\alpha u^2 + (6\gamma - 4\alpha\beta)u^4]v. \end{aligned} \tag{2}$$

The universal unfolding of the first kind for normal form (2) can be written as

$$\begin{aligned} \dot{u} &= v, \\ \dot{v} &= \varepsilon_1 u + \varepsilon_2 v + \varepsilon_3 u^2 v + a_1 u^3 + b_2 u^4 v, \end{aligned} \tag{3}$$

where $\varepsilon_1 = \bar{\sigma}$, $\varepsilon_2 = 2\bar{\mu}$, $\varepsilon_3 = -2\alpha$, $a_1 = -3\beta/2$ and $b_2 = 6\gamma - 4\alpha\beta$. ε_1, ε_2 and ε_3 are the three unfolding parameters. It can be seen from equation (3) that homoclinic bifurcations can occur due to $a_1 < 0$.

It is easy to see from equations (3) that when $\bar{\sigma} < 0$, the only equilibrium solution of equations (3) is the trivial solution $(u, v) = (0, 0)$. The stability of the trivial solution can be determined from the Jacobian, given by

$$D_w F = \begin{bmatrix} 0 & 1 \\ \varepsilon_1 + 2\varepsilon_3 uv + 3a_1 u^2 + 4b_2 u^3 v & \varepsilon_2 + \varepsilon_3 u^2 + b_2 u^4 \end{bmatrix}, \tag{4}$$

where $w = (u, v)^{\mathrm{T}}$. When $\bar{\mu} < 0$ ($\bar{\mu} > 0$), the trivial singular point is a sink (source). On the line $\bar{\mu} = 0$, limit cycles (Hopf bifurcation) may bifurcate from the trivial zero solution. A classical Hopf bifurcation analysis shows that when $\bar{\mu} > 0$, the limit cycle is stable (supercritical). On the line $\bar{\sigma} = 0$, the trivial zero solution bifurcates into three solutions through a pitchfork bifurcation.

The order of Hopf bifurcation is determined by the index of the first non-zero Lyapunov coefficient. For example, if the first Lyapunov coefficient equals zero but the second Lyapunov coefficient is non-zero, then the system is called a Hopf bifurcation of order 2, or a degenerate Hopf bifurcation of codimension 2. The Hopf bifurcation of order 2 is unstable and may yield two families of limit cycles under a perturbation. When $\varepsilon_3 \neq 0$, i.e., $\alpha \neq 0$, the Hopf bifurcation is of order 1; while for $\varepsilon_3 = 0$ ($\alpha = 0$), the Hopf bifurcation is of order 2. In the region defined by $\bar{\mu} < 0$, $\alpha > 0$, there exist two families of limit cycles, one of these is unstable, located inside the stable one.

When $\bar{\sigma} > 0$, system (3) has three singular points: $q_0 = (0, 0)$ and $q_\pm = (\pm\sqrt{2\bar{\sigma}/3\beta}, 0)$. q_0 is a saddle point, and the characteristic equation of the two non-zero solutions $q_\pm$ is

$$\lambda^2 - \Delta_1 \lambda + 2\bar{\sigma} = 0, \tag{5}$$

where

$$\Delta_1 = 2\bar{\mu} - \frac{4\alpha\bar{\sigma}}{3\beta} + \frac{4(6\gamma - 4\alpha\beta)\bar{\sigma}^2}{9\beta^2}. \tag{6}$$

The two non-zero solutions are sink and source when $\Delta_1 < 0$ and $\Delta_1 > 0$ respectively. When $\Delta_1 = 0$, Hopf bifurcation occurs from the non-zero solutions. According to the above discussion, the Hopf bifurcations are codimension 2 when $\varepsilon_3 = 0$ (or $\alpha = 0$) which implies that $\Delta_1 = 0$. Therefore, it is known [31] that system (3) has a limit cycle for $\Delta_1 < 0$ because the second Lyapunov coefficient is non-zero. When $\Delta_1 > 0$, $\alpha > 0$, system (3) has two limit cycles. It follows from equation (6) that the equation for determining the bifurcation curve of Hopf bifurcation, denoted by (H) (similar notations introduced later for other bifurcations), is given by

$$\mu = \frac{2\alpha\bar{\sigma}}{3\beta} - \frac{2(6\gamma - 4\alpha\beta)\bar{\sigma}^2}{9\beta^2} \tag{7}$$

or

$$\alpha = \frac{48\gamma\bar{\sigma}}{24\beta + 32\beta\bar{\sigma}} + \frac{315\beta\bar{\mu}}{210\bar{\sigma} + 280\bar{\sigma}^2}. \tag{8}$$

In order to easily study homoclinic bifurcations, we introduce the following scale transformations:

$$u \to \varepsilon u,\ v \to \varepsilon^2 v,\ \varepsilon_1 \to \varepsilon^2\varepsilon_1,\ \varepsilon_2 \to \varepsilon^2\varepsilon_2,\ b_2 \to \frac{b_2}{\varepsilon^2},\ T_1 \to \frac{T_1}{\varepsilon}, \tag{9}$$

under which system (3) can be written as

$$\begin{aligned} \dot{u} &= v, \\ \dot{v} &= \varepsilon_1 u + a_1 u^3 + \varepsilon(\varepsilon_2 + \varepsilon_3 u^2 + b_2 u^4)v. \end{aligned} \tag{10}$$

When $\varepsilon = 0$, equations (10) become

$$\begin{aligned} \dot{u} &= v, \\ \dot{v} &= \varepsilon_1 u + a_1 u^3, \end{aligned} \tag{11}$$

which is a Hamiltonian system with the Hamiltonian function

$$H(u, v) = \tfrac{1}{2} v^2 - \tfrac{1}{2}\varepsilon_1 u^2 - \tfrac{1}{4} a_1^4 = h. \tag{12}$$

When $h = 0$, there exists a pair of homoclinic loops $\Gamma^0 = \{\Gamma^0_-(T_1) | T_1 \in \mathbf{R}\} \cup \{q_0\} \cup \{\Gamma^0_+(T_1) | T_1 \in \mathbf{R}\}$ consisting of a hyperbolic saddle $q_0 = (0, 0)$ and two homoclinic orbits $\Gamma^0_+(T_1)$ and $\Gamma^0_-(T_1)$ based at a hyperbolic saddle. The equations of the pair of homoclinic loops can be found as

$$\begin{aligned} u(T_1) &= \pm 2\sqrt{\frac{\bar{\sigma}}{3\beta}}\,\mathrm{sech}(\sqrt{\bar{\sigma}}T_1), \\ v(T_1) &= \mp \frac{2\bar{\sigma}}{\sqrt{3\beta}}\tanh(\sqrt{\bar{\sigma}}\,T_1)\,\mathrm{sech}(\sqrt{\bar{\sigma}}T_1). \end{aligned} \tag{13}$$

Because the perturbation term in system (10), $\varepsilon(\varepsilon_2 + \varepsilon_3 u^2 + b_2 u^4)v$, is a constant function which is independent of time T_1, the Melnikov function can be written as

$$\begin{aligned} M(\bar{\sigma}, \bar{\mu}, \alpha) &= \int_{-\infty}^{\infty} v(T_1)\,[\varepsilon_2 + \varepsilon_3 u^2(T_1) + b_2 u^4(T_1)]v(T_1)\,\mathrm{d}T_1 \\ &= \int_{-\infty}^{\infty} v^2(T_1)[2\bar{\mu} - 2\alpha u^2(T_1) + (6\gamma - 4\alpha\beta)u^4(T_1)]\,\mathrm{d}T_1 \\ &= \frac{16\bar{\mu}\bar{\sigma}^{3/2}}{9\beta} - \frac{128\alpha\bar{\sigma}^{5/2}}{135\beta^2} + \frac{1024(6\gamma - 4\alpha\beta)\bar{\sigma}^{7/2}}{2835\beta^3}. \end{aligned} \tag{14}$$

To preserve the homoclinic loops under a perturbations, it requires $M(\bar{\sigma}, \bar{\mu}, \alpha) = 0$, which determines a bifurcation curve for homoclinic bifurcation (HL),

$$\bar{\mu} = \frac{8\alpha\bar{\sigma}}{15\beta} - \frac{64(6\gamma - 4\alpha\beta)\bar{\sigma}^2}{315\beta^2}, \tag{15}$$

$$\alpha = \frac{48\gamma\bar{\sigma}}{21\beta + 32\beta\bar{\sigma}} + \frac{315\beta\bar{\mu}}{168\bar{\sigma} + 256\bar{\sigma}^2}. \tag{16}$$

To determine the order of the homoclinic loops, let $M(\bar{\sigma}, \bar{\mu}, \alpha) = M$. Then if there exist the degenerate conditions: $M = M' = \cdots = M^{(k-1)} = 0$ and $M^{(k)} = \pm\infty$, the homoclinic loops are said to be of order $(2k-1)$, whereas if $M = M' = \cdots = M^{(k-1)} = 0$, but $M^{(k)} \neq 0$ with $M^{(k)}$ finite, then the homoclinic loops are said to be of order $2k$.

3. SUBHARMONIC MELNIKOV FUNCTION, DEGENERATE BIFURCATIONS OF CODIMENSION-3 AND LIMIT CYCLES

To find the conditions of the multiple limit cycles of the generalized codimension-3 Lienard oscillator appearing and disappearing, we need to consider the number of zeros of subharmonic Melnikov function. Let $(\bar{u}(T_1), \bar{v}(T_1))$ represent the closed periodic orbits inside or outside the two homoclinic loops Γ^0, and assume that the Hamiltonian function is $H(\bar{u}, \bar{v}) = h$ with period $\bar{T}$. Then, the subharmonic Melnikov function can be described by

$$\begin{aligned} M(h) &= \int_0^{\mathrm{T}} \bar{v}(T_1)\{\dot{\bar{v}}(T_1)[\varepsilon_2 + \varepsilon_3\bar{u}^2(T_1) + b_2\bar{u}^4(T_1)]\}\,\mathrm{d}T_1 \\ &= \int_{H=h} (\varepsilon_2 v + \varepsilon_3 u^2 v + b_2 u^4 v)\,\mathrm{d}u. \end{aligned} \tag{17}$$

When the degenerate conditions $M(h) = M'(h) = \cdots = M^{(k-1)}(h) = 0$ are satisfied, the system can have a limit cycle of multiplicity k under a perturbation, which is unstable and may lead to k limit cycles [32].

Because $M(h)$ given in equation (17) is a complete elliptic integral, in order to find the number of zeros of equation $M(h) = 0$, we may apply the method given by

Petrov [33–35] to consider $M(h)$ and calculate some elliptic integrals. To achieve this, let

$$I_0 = \int_{H=h} v\,\mathrm{d}u, \quad I_1 = \int_{H=h} u^2 v\,\mathrm{d}u, \ldots, I_i = \int_{H=h} u^{2i} v\,\mathrm{d}u, \tag{18}$$

then $M(h)$ is a linear combination of the integrals I_i, and thus the integrals, I_0 and I_1. The coefficients of the integrals I_i are the polynomials in h. To make it easy to discuss the number of zeros of $M(h)$, we want to express $M(h)$ as a function of I_0 and I_1. To do this, first we need to express all I_i ($i \geqslant 2$) in terms of I_0 and I_i. Thus, consider the loop Γ_h defined by Γ_h: $h = \frac{1}{2} v^2 - \frac{1}{2}\varepsilon_1 u^2 - \frac{1}{4} a_1 u^4$. Suppose that the two intersection points of the loop Γ_h with the abscissa axis are defined respectively, by $a = a(h)$, $b = b(h)$. Further denote the half loop of Γ_a as $\Gamma_h^+ = \{(u, v) \in \Gamma_h | v > 0\}$; we can then find

$$v(u, h) = (2h + \varepsilon_1 u^2 + \tfrac{1}{2} a_1 u^4)^{1/2}. \tag{19}$$

At the points a and b, $v = 0$, equation (19) yields

$$h = -\tfrac{1}{2}\varepsilon_1 u^2 - \tfrac{1}{4} a_1 u^4. \tag{20}$$

Hence,

$$\int_{H=h} (\ )\,\mathrm{d}u = 2\int_a^b (\ )\,\mathrm{d}u, \tag{21}$$

and so

$$\begin{aligned}
I_i &= 2\int_a^b u^{2i} v\,\mathrm{d}u = \frac{2}{a_1}\int_a^b a_1 u^{2i} v\,\mathrm{d}u = \frac{2}{a_1}\int_a^b (a_1 u^{2i} - \varepsilon_1 u^{2i-2} + \varepsilon_1 u^{2i-2}) v\,\mathrm{d}u \\
&= \frac{2}{a_1}\int_a^b (a_1 u^{2i} + \varepsilon_1 u^{2i-2}) v\,\mathrm{d}u - \frac{\varepsilon_1}{a_1} I_{i-1} = \frac{2}{a_1}\int_a^b u^{2i-3} v \\
&\quad \times \mathrm{d}\left(\frac{1}{4} a_1 u^4 + \frac{1}{2}\varepsilon_1 u^2\right) - \frac{\varepsilon_1}{a_1} I_{i-1} \\
&= \frac{2}{a_1}\int_a^b u^{2i-3} v^2\,\mathrm{d}v - \frac{\varepsilon_1}{a_1} I_{i-1} = \frac{2}{a_1}\int_a^b u^{2i-3}\,\mathrm{d}\left(\frac{1}{3} v^3\right) - \frac{\varepsilon_1}{a_1} I_{i-1} \\
&= \frac{2}{3a_1}[u^{2i-3} v^3]_a^b - \frac{2(2i-3)}{3a_1}\int_a^b u^{2i-4} v^3\,\mathrm{d}u - \frac{\varepsilon_1}{a_1} I_{i-1} \\
&= -\frac{2(2i-3)}{3a_1}\int_a^b u^{2i-4}\left(2h + \varepsilon_1 u^2 + \frac{1}{2} a_1 u^4\right) v\,\mathrm{d}u - \frac{\varepsilon_1}{a_1} I_{i-1} \\
&= \frac{2i-3}{6} I_i - \frac{2i}{3a_1}\varepsilon_1 I_{i-1} - \frac{2(2i-3)}{3a_1} h I_{i-2}
\end{aligned}$$

which can be rewritten as

$$(2i+3) I_i = -\frac{4i}{a_1}\varepsilon_1 I_{i-1} - \frac{4(2i-3)}{a_1} h I_{i-2} \quad \text{for } i \geqslant 2. \tag{22}$$

Setting $i = 2$ in the above equation results in

$$I_2 = -\frac{4}{7a_1} hI_0 - \frac{8}{7a_1} \varepsilon_1 I_1. \tag{23}$$

Based on equations (22) and (23), we can obtain the following results: (a) let $P = I_1/I_0$, then P satisfies a Ricatti equation

$$4h\left(4h - \frac{\varepsilon_1^2}{a_1}\right) P' = 5\varepsilon_1 P^2 + 8hP + 4\frac{\varepsilon_1^2}{a_1} P + 4\frac{\varepsilon_1}{a_1} h; \tag{24}$$

and (b) I_0 and I_1 satisfy the Picard–Fuchs equations

$$I_0 = \frac{4}{3} hI_0' + \frac{1}{3} \varepsilon_1 I_1',$$

$$I_1 = -\frac{4\varepsilon_1}{15a_1} hI_0' + \frac{4}{5} hI_1' - \frac{4\varepsilon_1^2}{15a_1} I_1'. \tag{25}$$

To prove part (a), define $J_i(h) = \frac{1}{2} I_i(h)$, and integrate this equation along the loop Γ_h to obtain

$$J_i(h) = \int_a^b u^{2i} v \, \mathrm{d}u,$$

and then differentiating both sides of the above equation with respect to h results in

$$J_i'(h) = \int_a^b \frac{u^{2i}}{v} \, \mathrm{d}u.$$

Since

$$J_i = \int_a^b \frac{u^{2i} v^2}{v} \, \mathrm{d}u = \int_a^b \frac{u^{2i}(2h + \varepsilon_1 u^2 + \frac{1}{2} a_1 u^4)}{v} \, \mathrm{d}u = 2hJ_1' + \varepsilon_1 J_{i+1}' + \frac{1}{2} a_1 J_{i+2}', \tag{26}$$

using the method of integration by parts yields

$$\begin{aligned} J_i &= \int_a^b u^{2i} v \, \mathrm{d}u = \frac{1}{2i+1} [u^{2i+1} v]_a^b - \frac{1}{2i+1} \int_a^b u^{2i+1} \, \mathrm{d}v \\ &= -\frac{1}{2i+1} \int_a^b \frac{u^{2i+1}(\varepsilon_1 u + a_1 u^3)}{v} \, \mathrm{d}u = -\frac{1}{2i+1} (\varepsilon_1 J_{i+1}' + a_1 J_{i+2}'), \end{aligned}$$

that is,

$$(2i+1) J_i = -\varepsilon_1 J_{i+1}' - a_1 J_{i+2}'. \tag{27}$$

Eliminating J_{i+2}' from equations (26) and (27) gives

$$(2i+3) J_i = 4hJ_i' + \varepsilon_1 J_{i+1}'.$$

In particular, we have

$$3J_0 = 4hJ_0' + \varepsilon_1 J_1', \tag{28}$$

$$5J_1 = 4hJ_1' + \varepsilon_1 J_2'. \tag{29}$$

Next, differentiating equation (23) with respect to h yields

$$J_2' = -\frac{4}{7a_1} J_0 - \frac{4}{7a_1} hJ_0' - \frac{8}{7a_1} \varepsilon_1 J_1',$$

and then substituting the above equation into equation (29) gives

$$\begin{aligned} 5J_1 &= 4hJ_1' - \varepsilon_1 \left(\frac{4}{7a_1} J_0 + \frac{4}{7a_1} hJ_0' + \frac{8}{7a_1} \varepsilon_1 J_1' \right) \\ &= -\frac{4}{7a_1} \varepsilon_1 J_0 - \frac{4}{7a_1} h\varepsilon_1 J_0' + \left(4h - \frac{8}{7a_1} \varepsilon_1^2 \right) J_1'. \end{aligned} \tag{30}$$

Now solve equations (28) and (29) for J_0' and J_1' to obtain

$$4h\left(4h - \frac{\varepsilon_1^2}{a_1} \right) J_0' = 12hJ_0 - \frac{4\varepsilon_1^2}{a_1} J_0 - 5\varepsilon_1 J_1, \tag{31}$$

$$4h\left(4h - \frac{\varepsilon_1^2}{a_1} \right) J_1' = 20hJ_1 + \frac{4\varepsilon_1 h}{a_1} J_0. \tag{32}$$

Finally, by the definition $P(h) = I_1(h)/I_0(h)$, we have

$$\begin{aligned} P'(h) &= \frac{I_1'(h)I_0(h) - I_0'(h)I_1(h)}{I_0^2(h)} \\ &= \frac{I_0\left(20hI_1 + 4\dfrac{h\varepsilon_1}{a_1} I_0 \right) - I_1\left(12hI_0 - \dfrac{4\varepsilon_1^2}{a_1} I_0 - 5\varepsilon_1 I_1 \right)}{4h\left(4h - \dfrac{\varepsilon_1^2}{a_1} \right) I_0^2} \end{aligned}$$

which can be written as Ricatti equation (24) with the aid of definition $P(h) = I_1(h)/I_0(h)$.

To prove part (b), simply eliminating J_0 from equations (28) and (29) with the aid of equation (24) leads to the Picard–Fuchs equations (25).

By using equations (18) and (23), we may rewrite the Melnikov function $M(h)$ as

$$M(h) = \left(\varepsilon_2 - \frac{4b_2}{7a_1} h \right) I_0(h) + \left(\varepsilon_3 - \frac{8b_2}{7a_1} \varepsilon_1 \right) I_1(h), \tag{33}$$

and we can define a new function $\bar{M}(h)$, given by

$$\bar{M}(h) = \frac{M(h)}{I_0(h)} = \left(\varepsilon_2 - \frac{4b_2}{7a_1} h \right) + \left(\varepsilon_3 - \frac{8b_2}{7a_1} \varepsilon_1 \right) P(h). \tag{34}$$

Thus, we may consider the zeros of function $\bar{M}(h)$ instead of function $M(h)$. To study equation (34), we first investigate the characteristics and bifurcation

diagram of function $P(h)$, which is determined by the solutions of the following vector field:

$$\dot{h} = 4h\left(\frac{\varepsilon_1^2}{a_1} - 4h\right),$$

$$\dot{P} = -5\varepsilon_1 P^2 - 8hP - 4\frac{\varepsilon_1^2}{a_1}P - 4\frac{\varepsilon_1}{a_1}h. \tag{35}$$

The phase portrait of equation (35) can show the qualitative behavior of function $P(h)$.

From the above analysis, we know that system (1) can exhibit homoclinic loops for $h = 0$. When $h \in (-\bar{\sigma}^2/6\beta, 0)$, there exist closed periodic orbits around each of the two centers $(\pm\sqrt{2\bar{\sigma}/3\beta}, 0)$. When $h > 0$, there exist periodic orbits enclosing all the three singular points of system (1).

We describe the results obtained above more clearly as follows: the bifurcation diagrams of function $P(h)$ are composed of the five trajectories $\Omega_1, \Omega_2, \Omega_3, \Omega_4$ and Ω_5 of the vector field (35).

(I) When $h < -\bar{\sigma}^2/6\beta$, Ω_1 is the unstable separatrix of the saddle point $(\varepsilon_1^2/4a_1, -\varepsilon_1/a_1)$.
(II) Ω_2 is the saddle point $(\varepsilon_1^2/4a_1, -\varepsilon_1/a_1)$.
(III) When $h \in (-\bar{\sigma}^2/6\beta, 0)$, Ω_3 is the unstable separatrix of the saddle point $(\varepsilon_1^2/4a_1, -\varepsilon_1/a_1)$ which connects the saddle point $(\varepsilon_1^2/4a_1, -\varepsilon_1/a_1)$ and the node $(0, -4\varepsilon_1/5a_1)$.
(IV) Ω_4 is the stable node $(0, -4\varepsilon_1/5a_1)$.
(V) Ω_5 is a trajectory converging to Ω_4 as $t \to +\infty$ (or as $h \to 0_+$).

To find the singular point, simply setting $\dot{h} = \dot{P} = 0$ in equation (35) yields the following four parts:

$$\xi_1 = (0, 0), \quad \xi_2 = \Omega_4 = \left(0, -\frac{4\varepsilon_1}{5a_1}\right), \quad \xi_3 = \Omega_2 = \left(\frac{\varepsilon_1^2}{4a_1}, -\frac{\varepsilon_1}{a_1}\right),$$

$$\xi_4 = \left(\frac{\varepsilon_1^2}{4a_1}, -\frac{\varepsilon_1}{5a_1}\right),$$

and the stability of these singular points can be readily determined from the Jacobian matrix of equation (35), given by

$$B = \begin{bmatrix} \left(\dfrac{4\varepsilon_1^2}{a_1} - 32h\right) & 0 \\ -8P - \dfrac{4\varepsilon_1}{a_1} & -10\varepsilon_1 P - 8h - \dfrac{4\varepsilon_1^2}{a_1} \end{bmatrix}, \tag{36}$$

which in turn leads to the characteristic equation

$$\lambda^2 = (10\varepsilon_1 P + 40h)\lambda - \left(\frac{4\varepsilon_1^2}{a_1} - 32h\right)\left(10\varepsilon_1 P + 8h + \frac{4\varepsilon_1^2}{a_1}\right) = 0, \tag{37}$$

where $a_1 < 0$, $\varepsilon_1 > 0$. Then it is easy to show that ξ_1 and ξ_3 are hyperbolic saddle points, ξ_2 is a stable node, and ξ_4 is an unstable node.

More properties of function $P(h)$ are summarized below.

(1) When $h \in (-\bar{\sigma}^2/6\beta, 0)$, $\mathrm{d}P/\mathrm{d}h < 0$, $\mathrm{d}P/\mathrm{d}h\,(\varepsilon_1^2/4a_1) = -1/2\varepsilon_1$, and $\mathrm{d}P/\mathrm{d}h(0) = -\infty$.
(2) When $h > 0$, $\mathrm{d}P/\mathrm{d}h$ has an unique zero at $h = \bar{h}$, and $\mathrm{d}P/\mathrm{d}h < 0$ for $h < \bar{h}$ and $\mathrm{d}P/\mathrm{d}h > 0$ for $h > \bar{h}$.
(3) When $h \to +\infty$, $P(h) \to +\infty$.
(4) When $h \in [-\bar{\sigma}^2/6\beta, 0)$, $\mathrm{d}^2P/\mathrm{d}h^2 < 0$, while $\mathrm{d}^2P/\mathrm{d}h^2 > 0$ for $h > 0$ and $\mathrm{d}P/\mathrm{d}h \leqslant 0$.
(5) When $h \to +\infty$, $P(h) \sim kh^{1/2}$ for some $k > 0$.
(6) There exists a unique inflection point $h_0 > \bar{h}$ such that $\mathrm{d}^2P(h_0)/\mathrm{d}h^2 = 0$, and $\mathrm{d}^2P/\mathrm{d}h^2 < 0$ for $0 < h < h_0$ and $\mathrm{d}^2P/\mathrm{d}h^2 > 0$ for $h > h_0$.

The proof for the above results is essentially the same as the proofs given in references [20, 23, 36].

By using the above results we can plot the phase portrait of system (35), as shown in Figure 1. For a comparison, we have used a numerical method to study equation (35) and obtained the simulation results, given in Figure 2 which only shows the upper-half phase portrait of system (35). Figure 2(b) shows the local phase portrait of Figure 2(a). The parameter values and the initial conditions are chosen as follows: $\varepsilon_1 = 1$, $a_1 = -1$, $h(0) = 4{\cdot}9$, $P(0) = 3{\cdot}0$ for $h > 0$, and $h(0) = -0{\cdot}24$, $P(0) = 1{\cdot}0$ for $h < 0$. Comparison of Figures 1 and 2 indicates a good agreement between the theoretical predictions and the numerical simulation results. The characteristics of the phase portrait of system (35) is mainly determined by the quintic non-linear term in system (1).

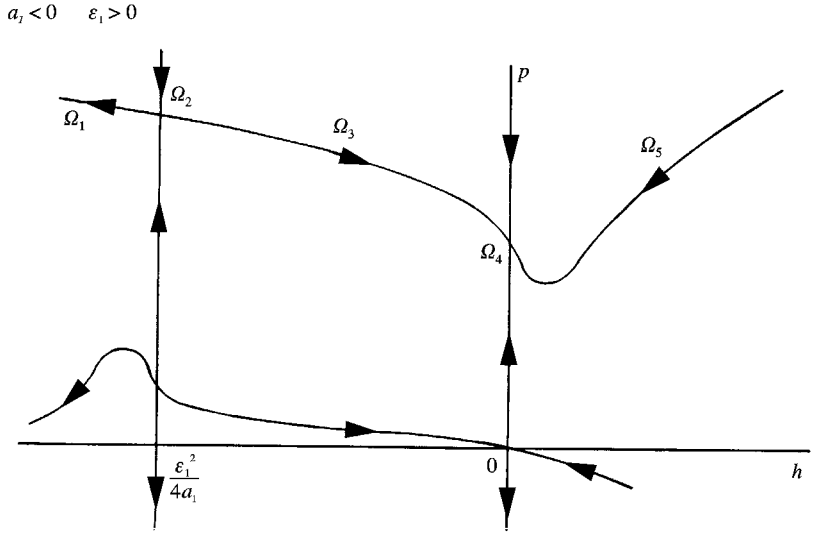

Figure 1. The phase portrait of system (35).

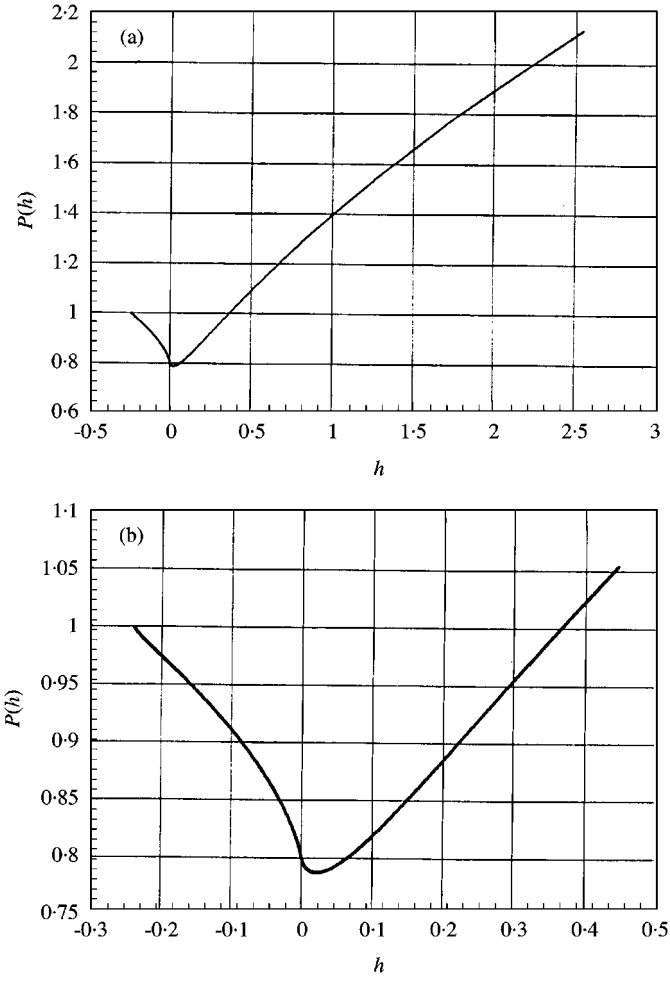

Figure 2. The numerical results for system (35): (a) the phase portrait; and (b) an enlarged window of part (a).

4. ANALYSIS ON THE DEGENERATE BIFURCATIONS OF CODIMENSION-3 AND LIMIT CYCLES

Having established results given in previous sections, we can now study the bifurcation diagram of the zeros of functions $M(h)$ or $\bar{M}(h)$. It follows from equation (34) and relation $\bar{M}(h) = 0$ that

$$P(h) = \frac{\varepsilon_2}{(8b_2/7a_1)\,\varepsilon_1 - \varepsilon_3} - \frac{(4b_2/7a_1)}{(8b_2/7a_1)\,\varepsilon_1 - \varepsilon_2}\, h. \tag{38}$$

Therefore, the zeros of $\bar{M}(h)$ can be determined by the intersection points of $P(h)$ with the line $\bar{M}(h) = 0$. Because $\bar{M}(h) = M(h)/I_0(h)$ and $I_0(h) \neq 0$, the number of the zeros of $\bar{M}(h) = 0$ equals the number of the zeros of $M(h)$. Figure 3 shows the

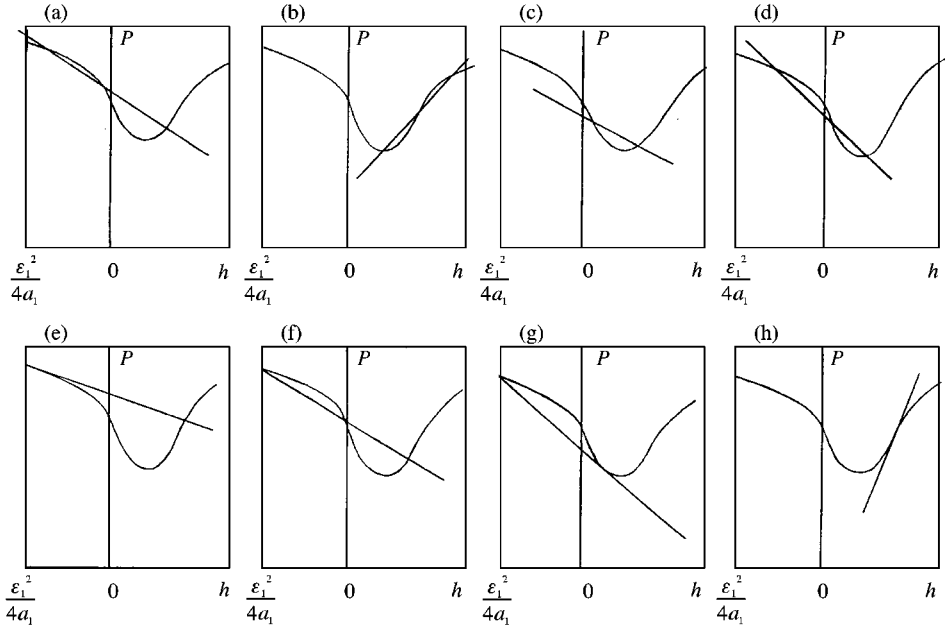

Figure 3. The curves of $\bar{M}(h) = 0$ and $P(h)$: (a) 2S and 1L LC; (b) 3L LC (c) 2L LC; (d) 1S and 2L LC; (e) (H_2); (f) (HL) and (H); (g) ($2C_{int}$); and (h) triple LC.

respective positions of $\bar{M}(h) = 0$ and $P(h)$ as well as the number of the zeros of $\bar{M}(h)$, where S, L, and LC respectively represent small, large and limit cycles. Based on Figure 3, we have the following observations.

(1) Figure 3(a) shows that two zeros of $M(h)$ are located in the interval $(-\bar{\sigma}^2/6\beta, 0)$. This suggests that two small limit cycles exist simultaneously, each of these containing one singular point, and one large limit cycle may also exist, enclosing all three singular points.
(2) Figure 3(b) indicates that $M(h)$ has three zeros in the interval $(0, +\infty)$. This implies that three large limit cycles can exist simultaneously, enclosing all the three singular points. In this case, no small limit cycles can occur.
(3) Figure 3(c) and 3(d) show that if there exist two large limit cycles, then at most only one small limit cycle may exist.
(4) Figure 3(e) shows that when the line $\bar{M}(h) = 0$ is tangent to $P(h)$ at the point $\Omega_2(\varepsilon_1^2/4a_1, -\varepsilon_1/a_1)$, a degenerate Hopf bifurcation of codimension 2 occurs. From the results obtained in the previous section, we know that the slope of the line $\bar{M}(h) = 0$ is $-1/(2\varepsilon_1)$, and then using equation (38) a point (H_2) for the degenerate Hopf bifurcation of codimension 2 is obtained as follows:

$$\varepsilon_2 = -\frac{b_2\varepsilon_1^2}{a_1^2}, \quad \varepsilon_3 = 0,$$

or

$$\bar{\mu} = -\frac{4\gamma\bar{\sigma}^2}{3\beta}, \quad \alpha = 0.$$

When the line $\bar{M}(h) = 0$ is tangent to $P(h)$ at the point $\Omega_4(0, -4\varepsilon_1/5a_1)$, there can be a symmetric homoclinic bifurcation of order 2. Because the slope of the line $\bar{M}(h) = 0$ at the point Ω_4 is ∞, we can use equation (38) to find a point (HL_2) for the degenerate homoclinic bifurcation of codimension 2:

$$\varepsilon_3 = \frac{8b_2}{7a_1}\varepsilon_1 \quad \text{or} \quad \alpha = \frac{48\gamma\bar{\sigma}}{21\beta + 32\beta\bar{\sigma}}.$$

(5) If the line $\bar{M}(h) = 0$ passes through the two points Ω_2 and Ω_4 simultaneously, there can exist a point at which a Hopf bifurcation and a symmetric homoclinic loop bifurcation occur simultaneously, as shown in Figure 3(f). In this case there is only one large limit cycle enclosing the symmetric homoclinic loop. Because the slope of the line $\bar{M}(h) = 0$ is $-4/5\varepsilon_1$, we can obtain the equations of a line and a curve from equation (38) as follows:

$$\varepsilon_3 = \frac{3b_2\varepsilon_1}{7a_1} \quad \text{and} \quad \varepsilon_2 = -\frac{4b_2\varepsilon_1^2}{7a_1}.$$

(6) Figure 3(g) shows that the line $\bar{M}(h) = 0$ is tangent to $P(h)$ and passes through the point Ω_2. Therefore, there exists a bifurcation point at which a double large limit cycle splits into two large limit cycles under a perturbation.

(7) The bifurcation curve ($2C_{int}$) for the two small limit cycles connects points (H_2) and (HL_2), while the bifurcation curve ($2C_{ext}$) for the two large limit cycles joints point (HL_2) and crosses the Hopf bifurcation curve (H).

(8) Figure 3(h) shows that the line $\bar{M}(h) = 0$ passes through the inflection point $h = h_0$. This suggests that there exists a bifurcation point from which a triple limit cycle can bifurcate.

Numerical results are given in Figure 4 to show the line $\bar{M}(h) = 0$ together with function $P(h)$ for the case of having three large limit cycles simultaneously. The parameter values used are $\varepsilon_1 = 1{\cdot}0$, $\varepsilon_2 = 2{\cdot}16$, $\varepsilon_3 = -0{\cdot}79541$, $a_1 = -1{\cdot}0$ and $b_2 = -1{\cdot}0$. The initial conditions used for the simulation are $h(0) = 4{\cdot}9$, $P(0) = 3{\cdot}0$ for $h > 0$, and $h(0) = -0{\cdot}24$, $P(0) = 1{\cdot}0$ for $h > 0$. Good agreement between the theoretical predictions and the numerical results has been observed from Figures 3 and 4.

It follows from equations (8) and (16) that the bifurcation curves for (H) and (HL) pass through points (H_2) and (HL_2) respectively. In the case of degenerate bifurcations of codimensions 3, the bifurcation diagram should be depicted in the three-dimensional parameter space ($\bar{\sigma}$, $\bar{\mu}$, α). Due to the complex relation between the parameters, it is difficult to draw accurate bifurcation surfaces and curves in the three-dimensional parameter space. So, we may use a set of bifurcation diagrams given in plane ($\bar{\mu}$, α); each of these corresponds to a fixed value of $\bar{\sigma}$.

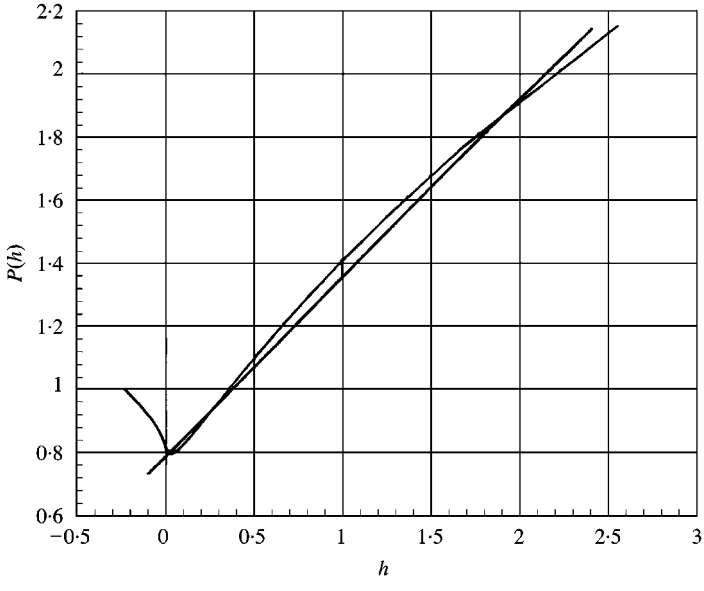

Figure 4. The numerical plotting for $\bar{M}(h) = 0$ and $P(h)$ in the case of three large limit cycles.

Based on the above analysis, we can now qualitatively draw the degenerate bifurcations of codimension 3 and the global bifurcations for the generalized Lienard oscillator (1) in plane $(\bar{\mu}, \alpha)$, as shown in Figure 5, where only the limit cycles are shown. The notations used in Figure 5 are: (HL_2), the point of degenerate homoclinic bifurcation of codimension 2, (H_2), the point of degenerate Hopf bifurcation of codimension 2, $(2C_{ext})$, the curve for the bifurcation of two large limit cycles, $(2C_{int})$, the curve for the bifurcation of two small limit cycles, (HL), the curve for the bifurcation of the homoclinic loop, and (H), the curve of Hopf bifurcation. Note that the coexistence of the multiple attractors for the limit cycle of the generalized Lienard equations (1) is seen in Figure 5.

5. HETEROCLINIC BIFURCATIONS

In this section, we turn to the case when $\bar{\sigma} < 0$ and $\beta < 0$. By letting $x = y_1$, $\dot{x} = y_2$, we obtain the universal unfolding of the first kind for the generalized Lienard oscillator (1) as follows:

$$\begin{aligned} \dot{y}_1 &= y_2, \\ \dot{y}_2 &= \varepsilon_1 y_1 + \varepsilon_2 y_2 + \varepsilon_3 y_1^2 y_2 + a_1 y_1^3 + b_2 y_1^4 y_2, \end{aligned} \tag{39}$$

where $\varepsilon_1 = -\bar{\sigma}$, $\varepsilon_2 = 2\bar{\mu}$, and $\varepsilon_3 = b_1 = -2\alpha$ are the three unfolding parameters, $a_1 = -3\beta/2$ and $b_2 = 6\gamma - 4\alpha\beta$ are constants. Due to $a_1 > 0$, system (39) can exhibit heteroclinic bifurcations.

When $\bar{\sigma} < 0$, the trivial zero solution of system (39) is the only singular (saddle) point. On the line $\bar{\sigma} = 0$, there is a Pitchfork bifurcation. When $\bar{\sigma} > 0$ there are

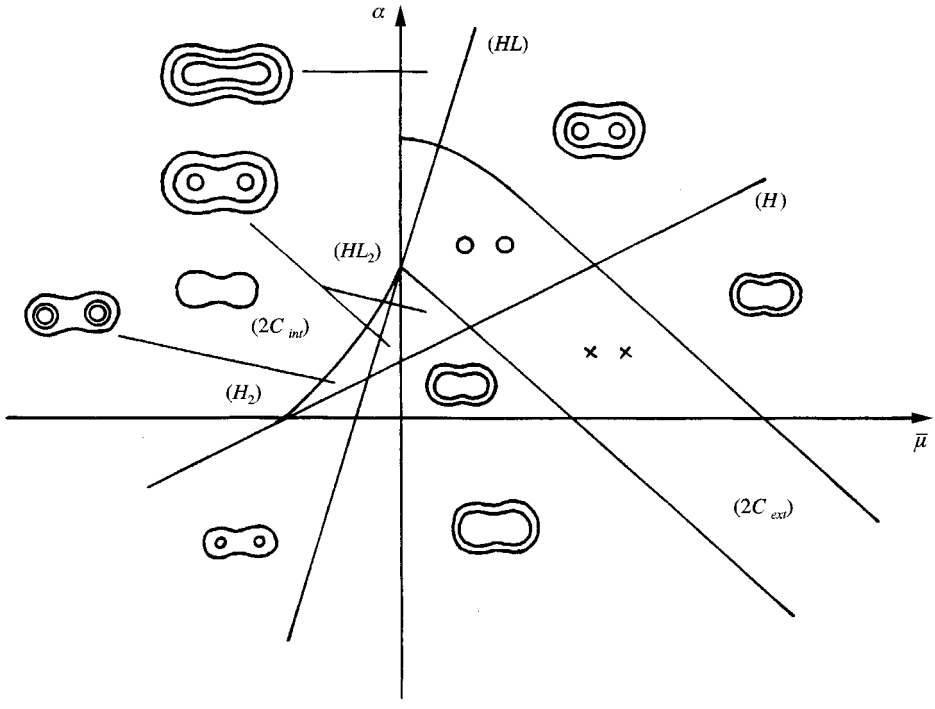

Figure 5. The bifurcation sets and phase portraits in plane $(\bar{\mu}, \alpha)$.

three singular points, given by $q_{\pm} = (\pm\sqrt{2\bar{\sigma}/3\beta}, 0)$ which are saddles, and $q_0 = (0, 0)$ which is a sink (source) when $\bar{\mu} < 0$ ($\bar{\mu} > 0$). On the line $\bar{\mu} = 0$, the zero solution bifurcates into a family of limit cycles which is stable for $\bar{\mu} > 0$. The Hopf bifurcation is of order 1 when $\varepsilon_3 \neq 0$, and is of order 2 when $\varepsilon_3 = 0$. Inside the region defined by $\bar{\mu} < 0$ and $\alpha < 0$, there exist two limit cycles.

In order to study heteroclinic bifurcations, we introduce the scale transformations

$$y_1 \to \varepsilon y_1, \quad y_2 \to \varepsilon^2 y_2, \quad \varepsilon_1 \to \varepsilon^2 \varepsilon_1, \quad \varepsilon_2 \to \varepsilon^2 \varepsilon_2, \quad b_2 \to \frac{b_2}{\varepsilon^2}, \quad T_1 \to \frac{T_1}{\varepsilon} \tag{40}$$

under which system (41) becomes

$$\begin{aligned} \dot{y}_1 &= y_2, \\ \dot{y}_2 &= \varepsilon_1 y_1 + a_1 y_1^3 + \varepsilon(\varepsilon_2 + \varepsilon_3 y_1^2 + b_2 y_1^4) y_2. \end{aligned} \tag{41}$$

Setting $\varepsilon = 0$ in equations (39) yields the Hamiltonian system

$$\begin{aligned} \dot{y}_1 &= y_2, \\ \dot{y}_2 &= \varepsilon_1 y_1 + a_1 y_1^3 \end{aligned} \tag{42}$$

with the Hamiltonian function

$$H(y_1, y_2) = \tfrac{1}{2} y_2^2 - \tfrac{1}{2}\varepsilon_1 y_1^2 - \tfrac{1}{4} a_1 y_1^4 = h. \tag{43}$$

When $H = \bar{\sigma}^2/6\beta$, there exists a heteroclinic loop $\Gamma^0 = \{q_-\} \cup \{P^0(T_1)\} \cup \{q_+\}$, which consists of the hyperbolic saddle $q_\pm$ and a pair of heteroclinic orbits $P^0(T_1)$ based at the saddles. The equations of the pair of heteroclinic orbits can be found as

$$\begin{aligned} y_1(T_1) &= \pm \sqrt{\frac{2\bar{\sigma}}{3\beta}} \tanh\left(\frac{\sqrt{2\bar{\sigma}}}{2} T_1\right), \\ y_2(T_1) &= \pm \frac{\bar{\sigma}}{\sqrt{3\beta}} \operatorname{sech}^2\left(\frac{\sqrt{2\bar{\sigma}}}{2} T_1\right). \end{aligned} \tag{44}$$

Because the perturbation term in equation (41), $\varepsilon(\varepsilon_2 + \varepsilon_3 y_1^2 + b_2 y_1^4) y_2$, is a constant function, independent of time T_1, the Melnikov function for the heteroclinic orbits is given by

$$\begin{aligned} M(\bar{\sigma}, \bar{\mu}, \alpha) &= \int_{-\infty}^{\infty} y_2(T_1)[\varepsilon_2 + \varepsilon_3 y_1^2(T_1) + b_2 y_1^4(T_1)]\, y_2(T_1)\, \mathrm{d}T_1 \\ &= \int_{-\infty}^{\infty} y_2^2(T_1)[2\bar{\mu} - 2\alpha y_1^2(T_1) + (6\gamma + 4\alpha\beta) y_1^4(T_1)]\, \mathrm{d}T_1 \\ &= \frac{8\sqrt{2}\bar{\sigma}^{3/2}\bar{\mu}}{9\beta} - \frac{16\sqrt{2\bar{\sigma}}^{5/2}\alpha}{135\beta^2} - \frac{512\sqrt{2}\bar{\sigma}^{7/2}(6\gamma + 4\alpha\beta)}{2835\beta^3}. \end{aligned} \tag{45}$$

To keep the heteroclinic loop preserved under a perturbation, it is necessary and sufficient that $M(\bar{\sigma}, \bar{\mu}, \alpha) \equiv 0$. Thus, a bifurcation curve (HL) for the heteroclinic bifurcation can be solved from equation (45) as

$$\alpha = -\frac{102\gamma\bar{\sigma}}{21\beta + 68\beta\bar{\sigma}} + \frac{315\beta}{2(21\bar{\sigma} + 68\bar{\sigma}^2)}\bar{\mu} \tag{46}$$

or

$$\bar{\mu} = \frac{2\alpha}{15\beta}\bar{\sigma} + \frac{64(6\gamma + 4\alpha\beta)}{315\beta^2}\bar{\sigma}^2. \tag{47}$$

In order to study the bifurcations of the subharmonic orbits and limit cycles, we need to find the subharmonic Melnikov function and may follow the procedure in analyzing the existence of the homoclinic loops. Thus, the value $h = 0$ corresponds to the origin of system (39). When $h = \bar{\sigma}^2/6\beta$, there exists a heteroclinic loop, and when $h \in (0, \bar{\sigma}^2/6\beta)$, there exist closed periodic orbits enclosing the origin of system (41). The qualitative diagram of function $P(h)$ can also be determined by the phase portraits of equation (35). Similar to the results presented in section 3, we have the following results.

The diagrams of function $P(h)$ consist of the five trajectories Q_1, Q_2, Q_3, Q_4, and Q_5 of the vector field (35) for $a_1 > 0$ and $\varepsilon_1 > 0$.

(1) When $h > \bar{\sigma}^2/6\beta$, Q_1 is a stable trajectory converging to the node $(\varepsilon_1^2/4a_1, -\varepsilon_1/5a_1)$ as $t \to +\infty$.
(2) Q_2 is the node $(\varepsilon_1^2/4a_1, -\varepsilon_1/5a_1)$.

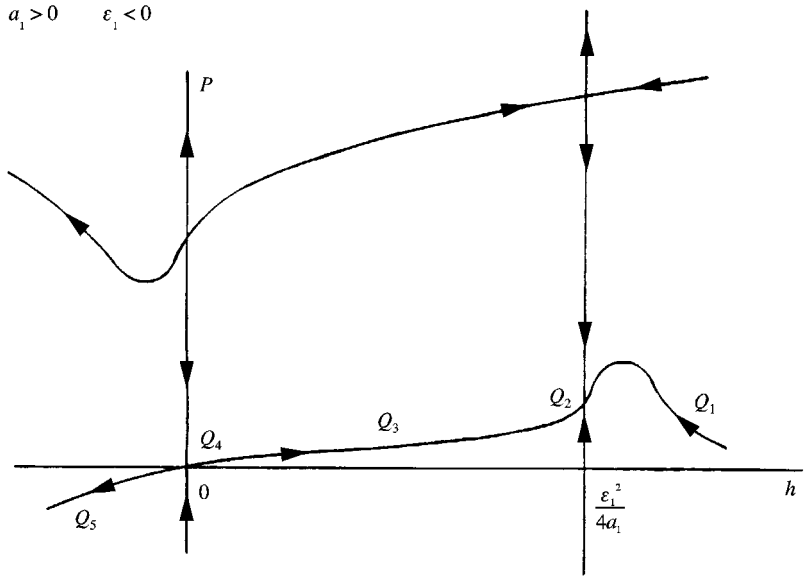

Figure 6. The phase portrait of system (35) for $a_1 > 0$ and $\varepsilon_1 < 0$.

(3) When $h \in (0, \bar{\sigma}^2/6\beta)$, Q_3 is a stable trajectory converging to node Q_2 and connects node Q_2 and the saddle point (0, 0).
(4) Q_4 is the saddle point (0, 0).
(5) Q_5 is the unstable separatrix of the saddle point (0, 0).

In the case of heteroclinic bifurcations, since $h \in [0, \bar{\sigma}^2/6\beta]$, we only need to use the diagrams of function $P(h)$ for $h \in [0, \bar{\sigma}^2/6\beta]$. Furthermore, the characteristic of function $P(h)$ for $h \in [0, \bar{\sigma}^2/6\beta]$ can be found as follows. When $h \in [0, (\bar{\sigma}^2/6\beta))$, $dP/dh > 0$, $dP/dh\,(h = 0) = -1/2\varepsilon_1$, $d^2P/dh^2 > 0$ and $dP/dh\,(\varepsilon_1^2/4a_1) = -\infty$.

Now we can use the above results to plot the function $P(h)$, as shown in Figure 6. Comparing the results with those obtained in section 3 shows that in the case of homoclinic bifurcations the function $P(h)$ is symmetric about the P-axis but not for the heteroclinic bifurcations. In the case of heteroclinic bifurcations we may use the lower half phase portrait given in Figure 6 to study limit cycles, while in the case of homoclinic bifurcations we may apply the upper half phase portrait given in Figure 1 to consider limit cycles.

Next, we study the bifurcation diagram of $\bar{M}(h) = 0$. Figure 7 shows the functions $\bar{M}(h)$ and $P(h)$, and the number of the zeros of $\bar{M}(h)$. The following properties are observed from Figure 7.

(1) Figure 7(a) shows that there is one zero of $\bar{M}(h)$ located in the interval $(0, \bar{\sigma}^2/6\beta)$, indicating that system (39) has one limit cycles enclosing the singular point (0, 0).
(2) From Figure 7(b) it is seen that there are two zeros of $\bar{M}(h)$ in the interval $(0, \bar{\sigma}^2/6\beta)$, and therefore at most two limit cycles may exist, enclosing the singular point (0, 0).

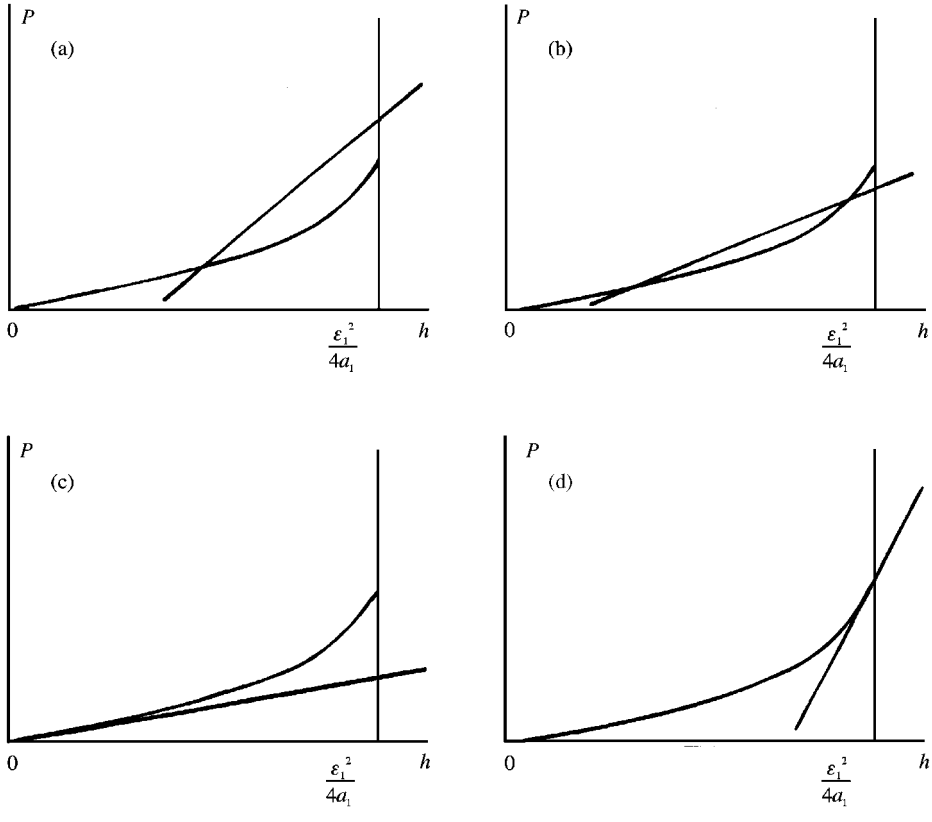

Figure 7. The curve of $\bar{M}(h) = 0$ and $P(h)$ for $a_1 > 0$ and $\varepsilon_1 < 0$: (a) 1 LC; (b) 2 LC; (c) (H_2); and (d) (HL_2).

(3) If the line $\bar{M}(h) = 0$ is tangent to $P(h)$ at the singular point $(0, 0)$, the degenerate Hopf bifurcation of codimension 2 can occur, as shown in Figure 7(c). Then by using the results obtained in the previous section we can find that the slope of $\bar{M}(h) = 0$ equals $(-1/2\varepsilon_1)$. Therefore, point (H_2) corresponding to the degenerate Hopf bifurcation of codimension 2 obtained from equation (38) is given by $\varepsilon_2 = 0$ and $\varepsilon_3 = 0$, or $\bar{\mu} = \alpha = 0$. When the line $\bar{M}(h) = 0$ is tangent to $P(h)$ at point $Q_2(\varepsilon_1^2/4a_1, -\varepsilon_1/5a_1)$, the degenerate heteroclinic bifurcation of codimension 2 can occur. Because the slope of line $\bar{M}(h) = 0$ is ∞, point (HL_2) associated with the degenerate heteroclinic bifurcation can be found from equation (38) as follows:

$$\varepsilon_3 = \frac{8b_2}{7a_1}\varepsilon_1 \quad \text{or} \quad \alpha = \frac{48\gamma\bar{\sigma}}{21\beta - 32\beta\bar{\sigma}}.$$

The above results can be used to qualitatively plot the bifurcation set of the degenerate bifurcations of codimension 3 for system (41) in the plane $(\bar{\mu}, \alpha)$, as

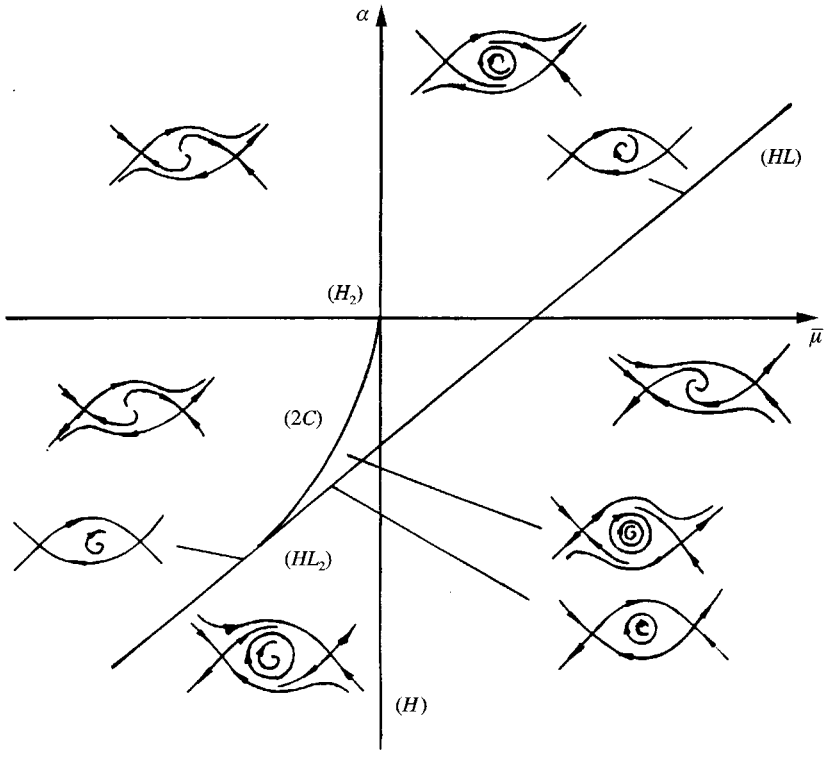

Figure 8. The bifurcation sets and phase portraits in plane $(\bar{\mu}, \alpha)$.

shown in Figure 8, where the notation (2C) denotes the bifurcation curve for the two limit cycles. Other notations are as defined in the previous section.

6. NUMERICAL SIMULATION

In order to verify the analytical results obtained in the previous sections, we have used a numerical method to investigate the degenerate bifurcations of codimension 3 and limit cycles. For simplicity, we only considered the case of the homoclinic bifurcations, in particular, the jumping phenomena. For comparison, we first summarize the analytical results below.

It has been shown that there co-exist multiple attractors of limit cycles in the generalized Lienard oscillator (1), and that the stability of the limit cycles can vary alternately. The periodic oscillations may jump from one limit cycle to another if the initial conditions are changed. The jumping phenomena are frequently observed in engineering and physical problems.

From the bifurcation diagram given in Figure 5 it is seen that the parameter plane $(\bar{\mu}, \alpha)$ can be divided into several regions, respectively corresponding to the existence of three large limit cycles, one small limit cycle and two large limit cycles, two large limit cycles, and two small limit cycles and one large limit cycle. It is also

observed that the jumping phenomena of oscillations can occur for the same parameter values. For example, in the region where there exist three large (external) limit cycles, the periodic oscillations of system (1) can jump from the smallest limit cycle to the largest limit cycle if the initial conditions are changed. In the region where one small limit cycle and two large limit cycles exist simultaneously, the periodic oscillations can jump from the small limit cycle to one of large limit cycles under the change of the initial conditions. For the stability behavior of multiple limit cycles, some of them may be stable and some of them unstable. For example, in the region where one small limit cycle and two large limit cycles exist simultaneously, one possibility is that the small limit cycle is unstable, the first large limit cycle is stable but the second large limit cycle is unstable. Another possibility is that the small limit is stable, the first large limit cycle is unstable but the second large limit cycle is stable. Thus, the periodic oscillations may jump from the stable limit cycle to the unstable limit cycle or to another stable limit cycle when the initial conditions are chosen appropriately.

To verify the above results, we used a numerical approach to study the universal unfolding (3). The numerical results are presented in Figures 9–16. Figures 9–11 show the coexistence of one small limit cycle and two large limit cycles. Figure 10 depicts an unstable large limit cycle, while Figure 11 shows that one unstable small limit cycle exists for each of the singular points. In Figures 9–11 the system parameters are chosen as follows:

$$\varepsilon_1 = 0{\cdot}2,\ a_1 = -2{\cdot}0,\ \varepsilon_2 = 1{\cdot}2,\ \varepsilon_3 = 12{\cdot}0,\ b_2 = 3{\cdot}5,\ \varepsilon = 0{\cdot}01.$$

There are, in a total, eight sets of the initial conditions. It is shown that the periodic oscillations can jump from the unstable small limit cycle to the stable large limit

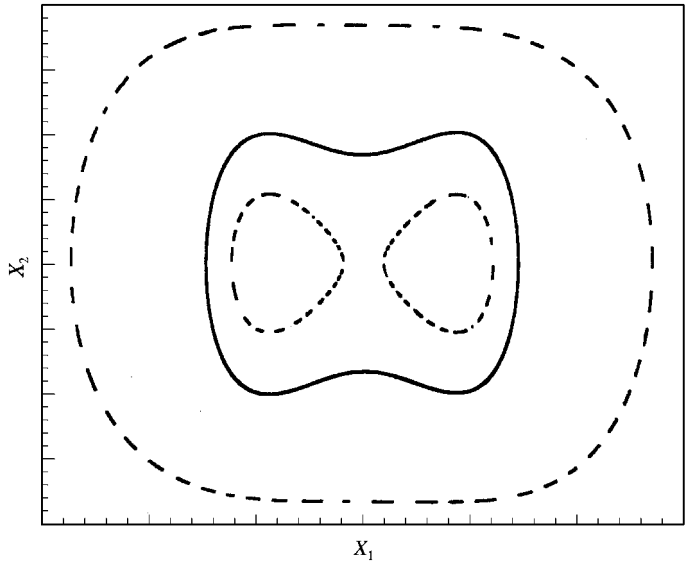

Figure 9. The coexistence of one small limit cycle and two large limit cycles.

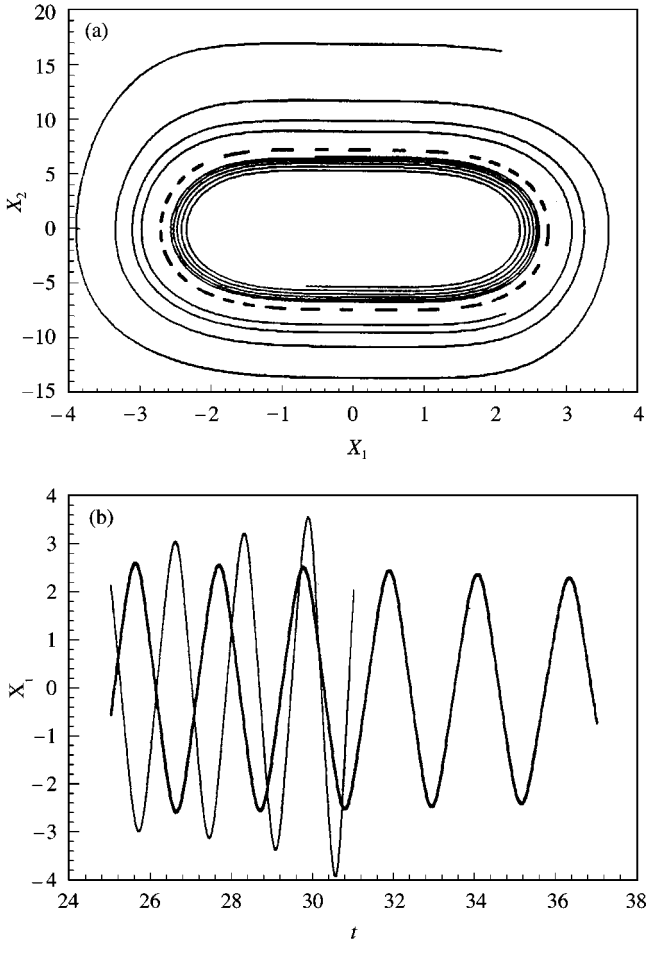

Figure 10. An unstable large limit cycle: (a) the phase portrait; and (b) the time history.

cycle, as well as to the unstable large limit cycle with variation of the initial conditions. This indicates a good agreement between the analytical prediction and the numerical simulation results.

Figures 12–14 show the coexistence of two large limit cycles. In particular, a stable large limit cycle is given in Figure 13 while an unstable large limit cycle is shown in Figure 14. The parameter values chosen in these figure are

$$\varepsilon_1 = 0{\cdot}2, a_1 = -2{\cdot}0, \varepsilon_2 = 1{\cdot}2, \varepsilon_3 = 6{\cdot}0, b_2 = 3{\cdot}5, \varepsilon = 0{\cdot}01.$$

There are five sets of the initial conditions. Again, it is seen that the periodic oscillations may jump from the stable large limit cycle to the unstable large limit cycle when the initial conditions are changed. This is also in a good agreement with the analytical results (Figure 5).

Additional numerical results are obtained for other regions, which are also in a good agreement with the analytical predictions. It is seen that given the same

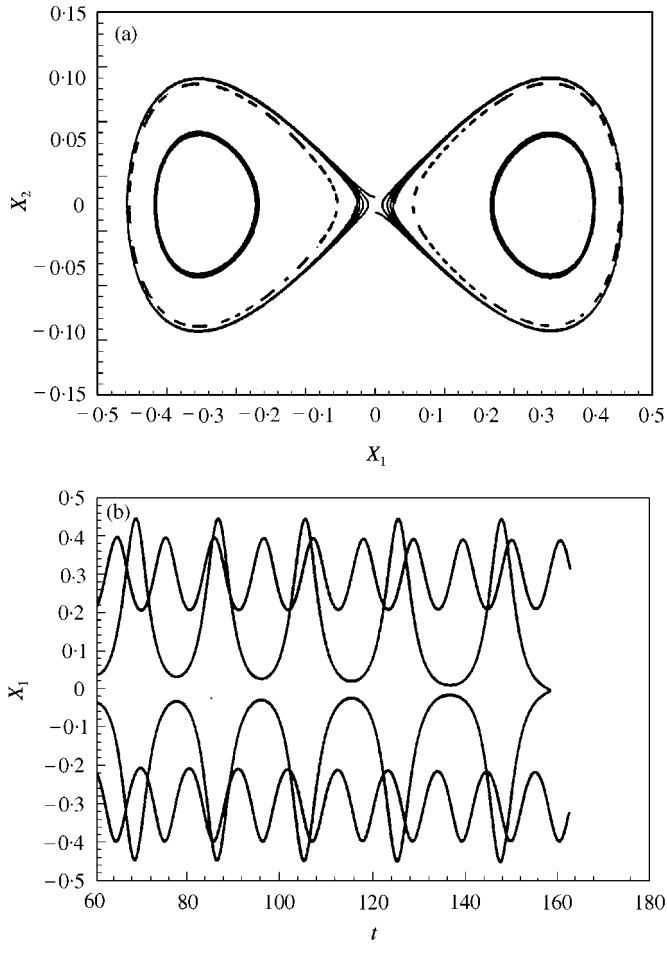

Figure 11. The coexistence of two large limit cycles: (a) the phase portrait, and (b) the time history.

parameter values, the periodic oscillations of the generalized Lienard oscillator can suddenly change if different initial conditions are chosen.

Moreover, it is observed from the numerical results that the jumping phenomenon can occur during the transition period. The oscillations first jump from the motion enclosing one singular point to the motion enclosing all three singular points, and finally converge to the stable periodic oscillations enclosing all three singular points. This motion order may be reversed, if appropriate parameter values are used. Figure 15 shows the jumping phenomenon in the transition period: the oscillations jump from the motion enclosing one singular point to the motion enclosing all the three singular points. The chosen system parameters are

$$\varepsilon_1 = 1{\cdot}0, a_1 = -0{\cdot}91, \varepsilon_2 = 1{\cdot}7, \varepsilon_2 = 1{\cdot}5, b_2 = 1{\cdot}8, \varepsilon = 0{\cdot}001,$$

$$u_0 = 0{\cdot}49, v_0 = 0{\cdot}37.$$

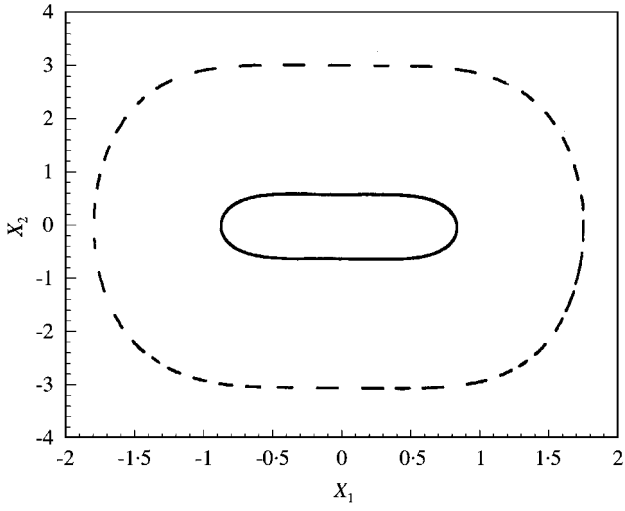

Figure 12. An unstable small limit cycle.

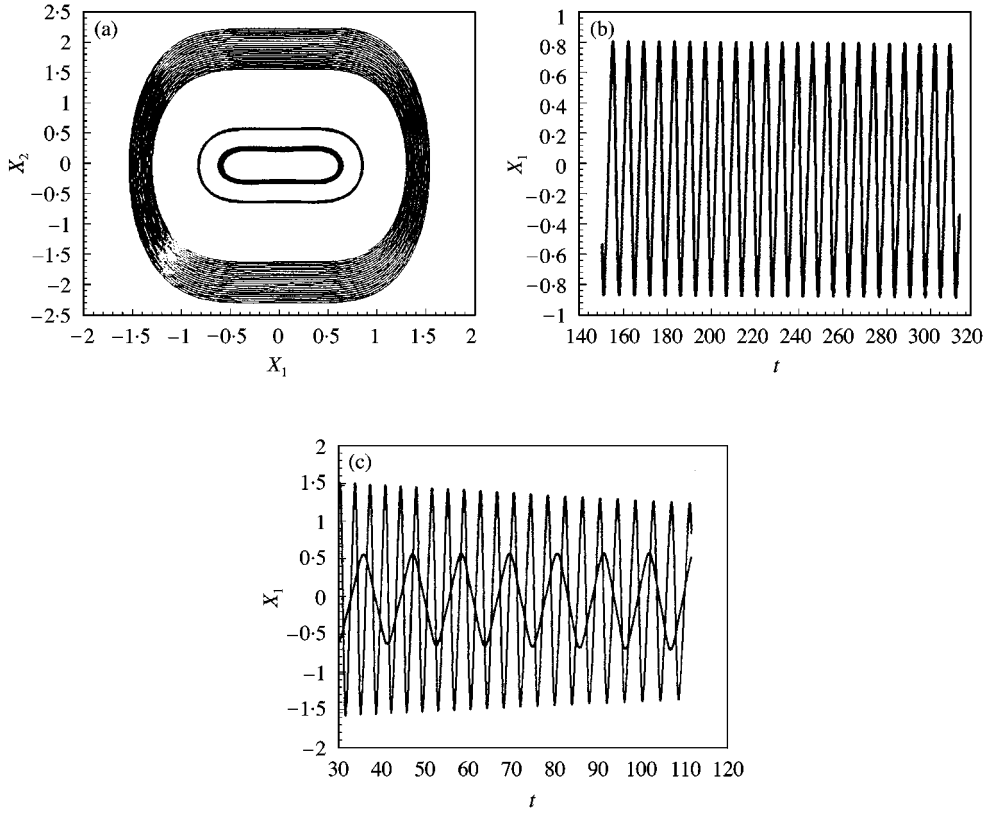

Figure 13. A stable large limit cycle: (a) the phase portrait; (b) the time history of the stable LC; and (c) two trajectories converging to the LC, one from outside and one from inside.

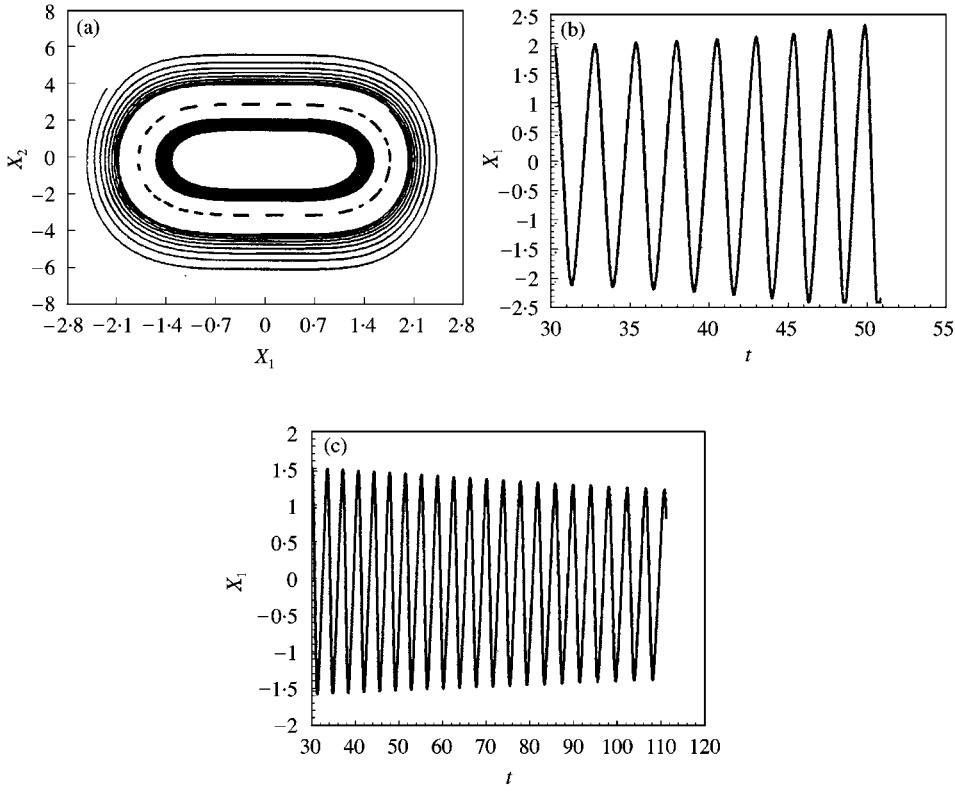

Figure 14. An unstable large limit cycle: (a) the phase portrait; (b) an orbit starting from outside of the unstable LC; (c) an orbit stating from inside of the unstable LC.

Figure 16 shows the jumping phenomenon during the transition period in the reverse order of Figure 15, with the following parameter values:

$$\varepsilon_1 = 1{\cdot}4, a_1 = -1{\cdot}25, \varepsilon_2 = 2{\cdot}1, \varepsilon_3 = 1{\cdot}8, b_2 = -1{\cdot}5, \varepsilon = 0{\cdot}01,$$

$$u_0 = -0{\cdot}65, v_0 = 0{\cdot}77.$$

7. CONCLUDING REMARKS

In this paper, a representative model—the generalized Lienard oscillator—is studied for the degenerate bifurcations of codimension 3 and limit cycles. Through the study, we have found the coexistence of the multiple limit cycles and the jumping phenomena from one periodic oscillation to another. The jumping phenomena are also found during the transition period. In particular, it has been shown that there limit cycles may exist simultaneously, which, to the best of our knowledge, has not been reported in the literature. The implication of the study given in the paper to physical problems is obvious. A very important aspect of

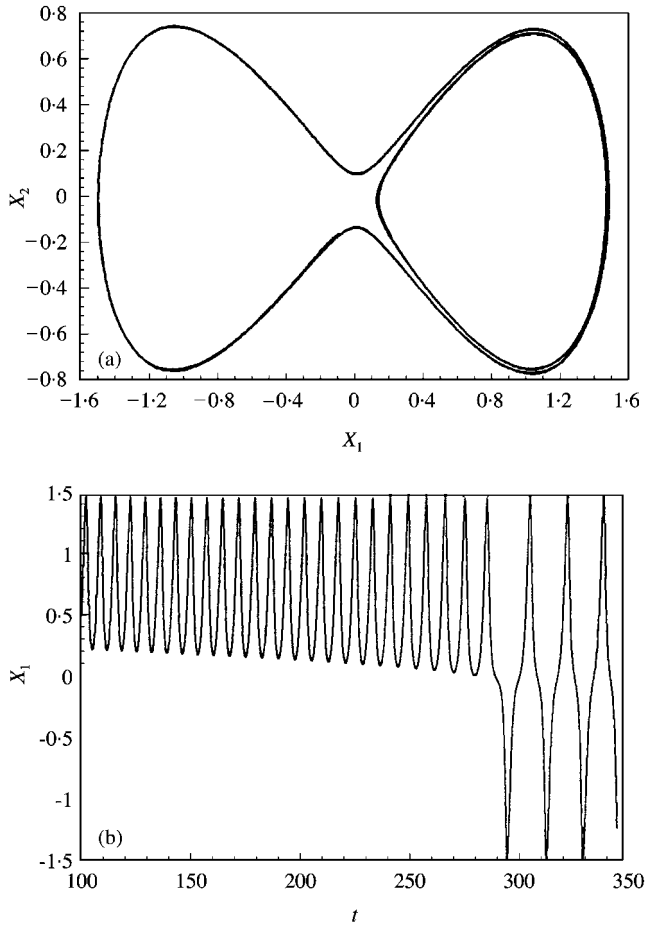

Figure 15. Transitional jumping phenomenon (I): (a) the phase portrait; and (b) the time history.

considering non-linear system is to control the system. To achieve this, one must understand its complex dynamics. For example, it has been known that machine tool chatter is usually caused by self-excited non-linear oscillations (limit cycles). The jumping phenomena between the limit cycles may suddenly change the state of machine tool and cause the damage of equipment. This shows the importance of studying higher codimension dynamical systems.

ACKNOWLEDGMENTS

The authors gratefully acknowledge the support of the Natural Science and Engineering Research Council of Canada. Zhang also thanks the support from the National Science Foundation of China. The help received from R. Wang is also acknowledged.

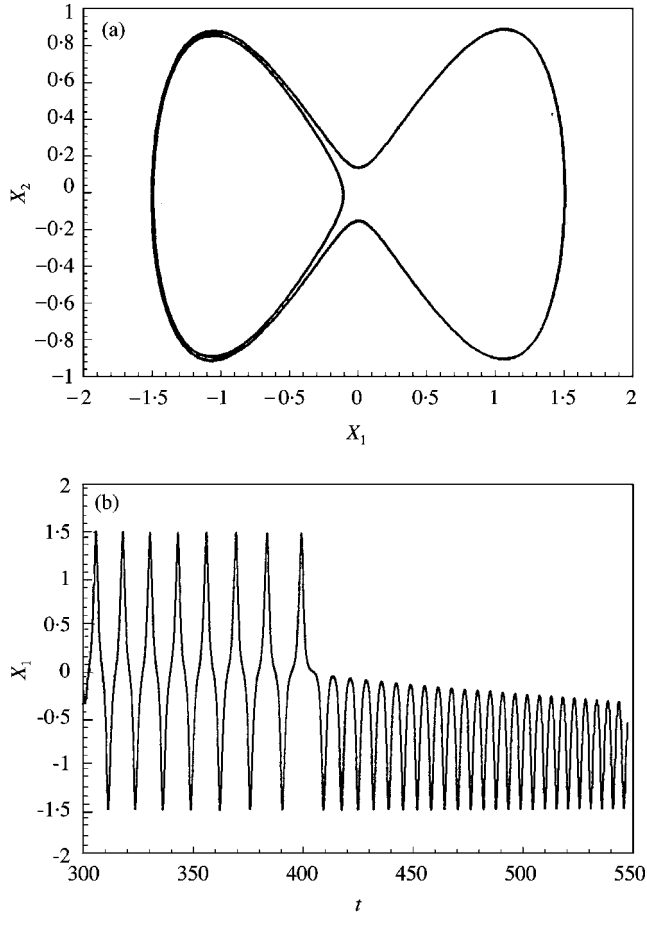

Figure 16. Transitional jumping phenomenon (II): (a) the phase portrait; and (b) the time history.

REFERENCES

1. F. C. Moon and M. A. Johnson 1998 *Dynamics and Chaos in Manufacturing Processes*, 3–32. (F. C. Moon, eds), New York: John Wiley & Sons. Nonlinear dynamics and chaos in manufacturing processes.
2. R. M. Corless and G. V. Parkinson 1988 *Journal of Fluids and Structures* **2**, 203–220. A model of the combined effects of vortex-induced vibration and galloping.
3. R. M. Corless and G. V. Parkinson 1993 *Journal of Fluids and Structures* **7**, 825–848. A model of the combined effects of vortex-induced vibration and galloping Part II.
4. P. Yu, A. H. Shah and N. Popplewell 1992 *ASME Journal of Applied Machines* **59**, 140–145. Inertially coupled galloping of iced conductors.
5. P. Yu, Y. M. Desai, A. H. Shah and N. Popplewell 1993 *ASME Journal of Engineering Mechanics* **119**, 2404–2425. Three-degree-of-freedom model for galloping, Part I: Formulation.
6. P. Yu, Y. M. Desai, N. Popplewell and A. H. Shah, 1993 *ASME Journal of Engineering Mechanics* **119**, 2426–2448. Three-degree-of-freedom model for galloping, Part II: solutions.

7. R. N. Arnold 1946 *Proceedings of the Institute of Mechanical Engineers* **154**, 261–284. The mechanism of tool vibration in the cutting of steel.
8. M. N. Hamdan and A. E. Bayoumi 1989 *Journal of Sound and Vibration* **128**, 451–469. An approach to study the effects of tool geometry on the primary chatter vibration in orthogonal cutting.
9. R. D. Blevins 1990 *Flow-Induced Vibration*. New York: Van Nostrand Reinhold Co., Seecond edition.
10. J. M. T. Thompson and H. B. Stewart 1986 *Nonlinear Dynamics and Chaos*. New York: Wiley.
11. H. Giacomini and S. Neukirch 1997 *Physical Review E* **56**, 3809–3813. Number of limit cycles of the Lienard equation.
12. M. A. F. Sanjuan 1998 *Physical Review E* **57**, 340–344. Lienard systems, limit cycles, and Melnikov theory.
13. R. E. Mickens 1988 *Journal of Sound and Vibration* **217**, 790–793. Lienard systems, limit cycles, Melnikov theory, and the method of slowly varying amplitude and phase.
14. J. Burnette and R. E. Mickens 1995 *Journal of Sound and Vibration* **188**, 298–300. The number of limit cycles for the generalized mixed Rayleigh–Lienard oscillator.
15. F. Takens 1973 *Annales de Institute Fourier* **23** 163–195. Normal forms for certain singularities of vector fields.
16. F. Takens 1974 *Publications de Mathematics IHES* **43**, 47–100. Singularities of vector fields.
17. F. Takens 1974 *Comm. Math. Inst*. **3**, Rijkuniversiteit Utrecht, 1–59, Forced oscillations and bifurcations.
18. R. I. Bogdanov 1975 *Functional Analysis and Its Applications* **9**, 144–145. Versal deformations of a singular point on the plane in the case of zero eigenvalues.
19. R. I. Bogdanov 1976 *Proceedings of Petrovskii Seminar* **2**, 23–35. Bifurcations of a limit cycle for a family of vector fields on the plane (English translation: Selecta Mathematics Formerly Sovietica 1 (1981), 373–388.) (in Russian).
20. F. Dumortier, R. Roussarie and J. Sotomayor 1987 *Ergodic Theory and Dynamical Systems* **7**, 375–413. Generic 3-parameter families of vector field on the lane, unfolding a singularity with nilpotent linear part. The cusp case.
21. F. Dumortier, R. Roussarie and J. Sotomayor 1990 *Preprint*. Generic 3-parameter families of planar vector fields, unfolding of saddle, focus and elliptic singularities with nilpotent linear parts.
22. C. Li and C. Rousseau 1989 *Journal of Differential Equation* **79**, 132–167. A system with three limit cycles appearing in a Hopf bifurcation and dying in a homoclinic bifurcation: the cusp of order 4.
23. C. Li and C. Rousseau 1990 *Canadian Journal of Mathematics* **XLII**, 191–212. Codimension 2 symmetric bifurcation and application to 1 : 2 resonance.
24. P. Joyal 1990 *Journal of Differential Equations* **88**, 1–14. The cusp of order N.
25. G. Dangelmayr and J. Guckenheimer 1987 *Archives Rational Mechanics and Analysis* **79**, 321–352. On a four parameter family of planar vector fields.
26. P. R. Sethna and S. W. Shaw 1987 *Physica D* **24**, 305–327. On codimension-three bifurcation in the motion of articulated tubes conveying a fluid.
27. Q. Bi and P. Yu 1999 *Journal of Computational and Applied Mathematics* **102**, 195–220. Symbolic computation of normal forms for semi-simple cases.
28. W. Zhang 1993 *Acta Mechanics Sinica* **25**, 548–559. Normal form and codimension three degenerate bifurcations in a nonlinear dynamical system.
20. Q. Bi and P. Yu 1998 *International Journal of Bifurcations and Chaos* **8**, 2279–2319. Computation of normal forms of differential equations associated with non-semisimple zero eigenvalues.
30. P. Yu and Q. Bi 1998 *Journal of Sound and Vibration* **217**, 691–736. Analysis of non-linear dynamics and bifurcations of a double pendulum.
31. S. L. Shi 1981. *Journal of Differential Equations* **41**, 301–312. A method of constructing cycles without contact around a weak focus.

32. Z. F. Zhang, T. R. Ding, W. Z. Huang and Z. X. Dong 1985 *Qualitative Theory of Differential Equations*. Beijing: Science Press.
33. G. S. Petrov 1984 *Functional Analysis & Applications* **18**, 148–150. Number of zeroes of complete elliptic integrals.
34. G. S. Petrov 1986 *Functional Analysis Applications* **20**, 37–40. Elliptic integrals and their nonoscillation.
35. G. S. Petrov 1987 *Functional Analysis Applications* **21**, 247–248. Complex zeroes of an elliptic integral.
36. C. Rousseau and H. Zoladak 1991 *Journal of Differential Equations* **94**, 41–54. Zeroes of complete elliptic integrals for 1:2 resonance.